Preliminary Mission Analysis for the 16U4SBSP Mission Concept

Boumchita, Wail; Feng, Jinglang; Clemente, Carmine; Vasile, Massimiliano; Busso, Caterina; Uludag, M.S.; Speretta, S.; Cervone, A.; Madi, Matteo

Publication date
2024

Document Version
Final published version

Published in
Proceedings of the 75th International Astronautical Conference

IAC-24-C2-IPB-11-x84758

Preliminary Mission Analysis for the 16U4SBSP Mission Concept.

Wail Boumchita[(1)], Jinglang Feng[(1)], Carmine Clemente[(1)], Massimiliano Vasile[(1)], Caterina Busso[(2)], Sevket Uludag[(3)], Stefano Speretta[(3)], Angelo Cervone[(3)], Matteo Madi[(4)]

[(1)] *University of Strathclyde, United Kingdom.*
[(2)] *Politecnico di Torino, Italy.*
[(3)] *TU Delft, The Netherlands.*
[(4)] *Sirin Orbital Systems AG, Switzerland.*

Abstract

The 16U4SBSP mission aims to demonstrate Space-Based Solar Power (SBSP) using a CubeSat (CS) swarm from Earth orbit. This mission employs seven 16U CSs to deliver 1 kW-scale wireless energy via Radio-Frequency (RF) beaming, adaptable for space-to-ground and space-to-space applications. The goal is to validate SBSP provision using a satellite swarm and to explore miniaturized technologies for future large-scale missions. A pre-Phase 0 study funded by the European Space Agency (ESA) through the Sysnova campaign has shown encouraging feasibility results. This paper presents a study on the formation flying and orbital dynamics of a CS mission, using a model that includes Earth's gravitational perturbations, solar radiation pressure (SRP), atmospheric drag, and lunar and solar gravity. The swarm configuration consists of seven CSs, with one at the center and six in a hexagonal arrangement. The Concept of Operations (CONOPS) is divided into three phases: deployment and acquisition, maintenance, and disposal. CSs are deployed at 30-second intervals, followed by a one-day Launch and Early Orbit Phase (LEOP) for subsystem checks. A 1000-meter formation is initially established, then reduced to 100 meters for the first half of the mission and 10 meters for the second half, maintained by a bang-bang limit-cycle controller. A disposal strategy compliant with ESA's Space Debris Mitigation Requirements is outlined. The analysis characterizes propellant consumption at various altitudes, proposes optimal initial conditions and launch dates, and performs a trade-off analysis, resulting in a detailed mission characterization and baseline definition. The work presented in the paper proves the feasibility of the 16U4SBSP mission, which would supply clean energy from space through wireless power transfer.

Keywords: Space-Based Solar Power, Formation flying, CubeSat mission, Sun-Synchronous Orbit

1 Introduction

16U4SBSP is a mission concept intended to perform a scaled in-orbit demonstration of SBSP. In this demonstration mission, a swarm of 7 identical 16U CSs is intended to provide wireless energy at power levels in the 1-kW scale (total amount of received power on the Earth's surface), using RF beaming. Although the mission is mainly intended for space-to-ground demonstrations, the spacecraft in the swarm are designed in such a way to also be suitable for space-to-space applications. The main objective of the mission is to validate the concept of providing SBSP by means of a swarm of satellites. At the same time, however, the mission is also intended as an in-orbit demonstration for a number of miniaturized technologies. The ultimate objective is to pave the way to full-scale missions which could serve users in remote areas with low power requirements or support emergency operations in blackout zones affected by unpredicted hazards. The mission therefore represents a low-cost precursor towards larger scale SBSP, where the actual transferred power would be in the GW range or larger, to supply clean and affordable energy to large areas on the Earth's surface. 16U4SBSP was one of the proposals submitted to the ESA SysNova challenge "Innovative Missions Concepts enabled by Swarms of CubeSats," aimed at generating new concepts for CS swarm missions in Earth orbit and quickly verifying their usefulness and feasibility through short concurrent studies [1]. After the initial phase of the challenge (open call for ideas), 16U4SBSP was selected as one of seven proposals for a Phase 0 analysis funded by ESA. This paper details the deployment, operational, and end-of-life strategies for the mission, discussing the formation flying techniques and dynamical models used to maintain the CSs under various orbital perturbations. The results confirm the feasibility of this innovative mission,

demonstrating successful deployment strategies, effective formation maintenance, and compliance with debris mitigation standards in its concluding phases—critical steps toward future large-scale SBSP missions.

2 Reference frames

2.1 ECI frame

The Earth-Centered Inertial (ECI) reference frame is used for describing the orbital motion of a spacecraft with respect to Earth. Its foundational characteristic is its inertial nature, meaning it does not rotate with the Earth but maintains a fixed orientation relative to the distant stars. The origin of the ECI frame is located at the Earth's center of mass, providing a geocentric perspective for space observation and analysis. The ECI coordinate system is defined by three orthogonal axes. The x-axis is aligned with the vernal equinox, creating a fixed direction in space that intersects the Earth's equatorial plane and the ecliptic plane. The y-axis extends perpendicularly from the x-axis within the equatorial plane, pointing towards the east. The z-axis is perpendicular to the Earth's equatorial plane, extending towards the North Pole, thus completing a right-handed coordinate system.

2.2 RTN frame

The Radial-Tangential-Normal (RTN) reference frame offers a localized view of object motion in orbit around the Earth. The RTN frame is used for describing the relative motion of spacecraft. Its axes are oriented based on the instantaneous position and velocity of a reference spacecraft or object. The RTN frame is defined by three axes oriented with respect to the direction of motion of the reference object. The Radial (R) axis points from the center of the Earth directly towards the object. The Tangential (T) axis lies in the plane of the object's orbit, pointing in the direction of its velocity vector. The Normal (N) axis is perpendicular to the orbital plane, pointing in the direction of the orbital angular momentum vector.

2.3 ECI to RTN conversion

Given a spacecraft's position $\mathbf{r}_{ECI}$ and velocity $\mathbf{v}_{ECI}$ vectors in the ECI frame, the transformation to the RTN frame involves the following steps [2].

1. **Radial Component $\hat{\mathbf{r}}$**: The radial unit vector is directed from the Earth's center towards the spacecraft, defined as
$$\hat{\mathbf{r}} = \frac{\mathbf{r}_{ECI}}{r_{ECI}} \tag{1}$$
2. **Tangential Component $\hat{\mathbf{t}}$**: The tangential unit vector is defined as the unit vector in the direction of the spacecraft's velocity vector, thus
$$\hat{\mathbf{t}} = \frac{\mathbf{v}_{ECI}}{v_{ECI}} \tag{2}$$
3. **Normal Component $\hat{\mathbf{n}}$**: The normal unit vector, perpendicular to the orbital plane, is obtained by the cross product of the radial and tangential vectors
$$\hat{\mathbf{n}} = \hat{\mathbf{r}} \times \hat{\mathbf{t}} \tag{3}$$
4. **Transformation Matrix**: The transformation matrix $\mathbf{A}$ can be formed using the unit vectors as columns
$$\mathbf{A} = \begin{bmatrix} \hat{\mathbf{r}} & \hat{\mathbf{t}} & \hat{\mathbf{n}} \end{bmatrix} \tag{4}$$
5. **Converting a Vector from ECI to RTN**: To transform a vector $\mathbf{x}_{ECI}$ from ECI to RTN frame, it is multiplied by the transpose of the transformation matrix
$$\mathbf{x}_{RTN} = \mathbf{A}^{\mathbf{T}}\mathbf{x}_{ECI} \tag{5}$$

3 Main perturbations

3.1 Gravitational perturbations

The Earth's gravitational potential is approximated using spherical harmonics. This method is based on the expansion of the gravitational potential in terms of spherical harmonics, which are a set of orthogonal functions defined on the surface of a sphere. The shape and density variations of Earth are represented by the Stokes coefficients. The gravitational potential V, in spherical harmonics expansion of degree n and order m, is given in spherical coordinates (r,δ,ϕ) as [3]

$$V = -\frac{\mu}{r} + \sum_{n=2}^{\infty}\sum_{m=0}^{n}\frac{\mu}{r}\left(\frac{R_e}{r}\right)^n P_{nm}(\sin\phi) \\ (C_{nm}\cos m\delta + S_{nm}\sin m\delta) \tag{6}$$

where ϕ and δ are the colatitude and the longitude, respectively. The perturbing acceleration is obtained as

$$\mathbf{a}_{nm} = -\nabla V \tag{7}$$

The zonal harmonics terms considered are from the 2^{nd} to 4^{th} degree and their respective coefficients are $J_2 = 0.00108263$, $J_3 = -2.5327 \times 10^{-6}$ and $J_4 = -1.6196 \times 10^{-6}$.

3.2 Solar radiation pressure perturbations

Solar radiation pressure, P_{SRP}, is expressed as [2]

$$P_{SRP} = \frac{S}{c} = \frac{1367\ \text{N}\cdot\text{m}^{-2}}{2.998 \times 10^8\ \text{m/s}} \approx 4.56 \times 10^{-6}\ \text{N/m}^2 \tag{8}$$

where S is the solar constant and c is the speed of light. The spacecraft surface is subdivided into n_f facets and the solar radiation pressure force acting on the spacecraft is computed as the sum of the forces acting on each single facet, i.e.

$$\mathbf{F}_{SRP} = \sum_{i=1}^{n_f} \mathbf{F}_{SRP,i}, \tag{9}$$

where $\mathbf{F}_{SRP,i}$ for each facet is given by

$$\mathbf{F}_{SRP,i} = -P_{SRP} S_i \left(c_{ai}\hat{\mathbf{u}} + c_{di}\hat{\mathbf{n}}_i + c_{si}\left(\hat{\mathbf{u}}\cdot\hat{\mathbf{n}}_i\right)\hat{\mathbf{n}}_i \max\left(\hat{\mathbf{u}}\cdot\hat{\mathbf{n}}_i, 0\right)\right) \tag{10}$$

where S_i is the surface area of each facet, $c_{ai} = 1 - \rho_i s_i$, with ρ_i the total reflectivity of the facet and s_i the fraction of ρ_i that is specular, $c_{si} = 2\rho_i s_i$, $c_{di} = \frac{2}{3} c_{ai}$, $\hat{\mathbf{u}}$ is the unit vector pointing from the spacecraft to the Sun and $\hat{\mathbf{n}}_i$ is the facet outer-pointing normal unit vector [4]. The perturbing acceleration is obtained as

$$\mathbf{a}_{SRP,i} = \frac{\mathbf{F}_{SRP,i}}{m} \tag{11}$$

where m is the spacecraft's mass.

3.3 Atmospheric drag perturbations

Atmospheric perturbation affects spacecraft motion significantly, particularly in LEO. The spacecraft velocity relative to the atmosphere v_{rel} is defined as

$$\mathbf{v}_{rel} = \mathbf{v} - \omega_E \times \mathbf{r} \tag{12}$$

where $\mathbf{v}$ is the spacecraft inertial velocity, ω_E is the Earth's angular velocity, and $\mathbf{r}$ is the radial position vector of the spacecraft. Similarly to the SRP perturbation, the atmospheric drag force acting on the spacecraft is computed as the sum of the forces acting on each single facet

$$\mathbf{F}_D = \sum_{i=1}^{n_f} \mathbf{F}_{D,i}, \tag{13}$$

where $\mathbf{F}_{D,i}$ for each facet is given by

$$\mathbf{F}_{D,i} = -\frac{1}{2} S_i C_D \rho v_{rel}^2 \max(\hat{\mathbf{n}}_s \cdot \frac{\mathbf{v}_{rel}}{v_{rel}}, 0) \tag{14}$$

where C_D is the drag coefficient, ρ is the atmospheric density and $\hat{\mathbf{n}}_s$ is the surface element outer-pointing unit normal vector [5]. The perturbing acceleration is obtained as

$$\mathbf{a}_{D,i} = \frac{\mathbf{F}_{D,i}}{m} \tag{15}$$

3.4 Third-body perturbations

Third bodies, such as the Sun and Moon, influence the dynamical evolution of the spacecraft around the Earth. The perturbation acceleration from these bodies is

$$\mathbf{a}_{TB} = -\mu_p \left[\frac{\mathbf{r} - \mathbf{d}}{(r-d)^3} + \frac{\mathbf{d}}{d^3}\right]. \tag{16}$$

where μ_p is the gravitational constant of the perturbing body, $\mathbf{r}$ signifies the position vector of the spacecraft with reference to Earth's center of mass, and $\mathbf{d}$ denotes the vector position of Earth's center of mass with respect to the disturbing celestial body [2].

4 Dynamical model

4.1 Orbit

4.1.1 Orbital elements

Classically, the orbit of a body is described by means of the Keplerian osculating elements: the semimajor axis a, the eccentricity e, the inclination i, the right ascension of the ascending node Ω, the argument of perigee ω and the true anomaly ν. The motion of spacecraft orbiting the Earth deviates from the Keplerian two-body problem due to various perturbative forces. These perturbations arise from multiple sources, including the non-spherical nature of the Earth's gravitational field, atmospheric drag, solar radiation pressure, and gravitational influences from the Moon and the Sun, as previously listed. To include these perturbations, the time variation of the osculating Keplerian elements can be analytically computed using the so-called Lagrange planetary equations of motion or, if non-conservative forces are acting on the system, the Gaussian planetary equations. However, both the Lagrangian and Gaussian equations of motion are subject to singularities, which present challenges when propagating orbits [6]. To avoid these difficulties, an alternative set of orbital parameters, known as equinoctial elements, is often employed. Equinoctial elements provide a non-singular representation of the orbit, enabling the continuous and accurate propagation of spacecraft trajectories under the influence of perturbative forces.

4.1.2 Equinoctial elements

The osculating equinoctial elements are the variables (a, P_1, P_2, Q_1, Q_2, Λ) [7], where

$$\begin{cases} P_1 &= e\sin(\Omega+\omega), \\ P_2 &= e\cos(\Omega+\omega), \\ Q_1 &= \tan\left(\frac{i}{2}\right)\sin\Omega, \\ Q_2 &= \tan\left(\frac{i}{2}\right)\cos\Omega, \\ \Lambda &= \nu+\omega+\Omega \end{cases} \tag{17}$$

4.1.3 Equations of Motion

When both conservative and non-conservative forces act on the spacecraft the time variation of the equinoctial elements is given by the Gaussian VOP. Expressed in terms of the equinoctial elements, the Gaussian variation equations of motion are

$$\begin{cases} \frac{da}{dt} &= -\frac{2}{\eta}\sqrt{\frac{a^3}{\mu_\oplus}}\left((P_2\sin\Lambda - P_1\cos\Lambda)f_R + \Phi f_T\right) \\ \frac{dP_1}{dt} &= \eta\sqrt{\frac{a}{\mu_\oplus}}\left(-\sin\Lambda f_R + \left(\frac{P_1+\sin\Lambda}{\Phi}+\sin\Lambda\right)\right. \\ &\qquad \left. f_T - \frac{P_2}{\Phi}Q_1\cos\Lambda - Q_2\sin\Lambda f_N\right), \\ \frac{dP_2}{dt} &= \eta\sqrt{\frac{a}{\mu_\oplus}}\left(\cos\Lambda f_R + \left(\frac{P_2+\cos\Lambda}{\Phi}+\cos\Lambda\right)\right. \\ &\qquad \left. f_T + P_1\frac{Q_1\cos\Lambda - Q_2\sin\Lambda}{\Phi}f_N\right), \\ \frac{dQ_1}{dt} &= \eta\frac{1}{2}\sqrt{\frac{a}{\mu_\oplus}}\left(1+Q_1^2+Q_2^2\right)\sin\Lambda\frac{f_N}{\Phi}, \\ \frac{dQ_2}{dt} &= \eta\frac{1}{2}\sqrt{\frac{a}{\mu_\oplus}}\left(1+Q_1^2+Q_2^2\right)\cos\Lambda\frac{f_N}{\Phi}, \\ \frac{d\Lambda}{dt} &= \sqrt{\frac{\mu_\oplus\Phi^2}{an^3}}\sqrt{\frac{a^3\eta}{\mu_\oplus\Phi}}\left(Q_1\cos\Lambda - Q_2\sin\Lambda\right)f_N \end{cases} \tag{18}$$

where $\eta = \sqrt{1-P_1^2-P_2^2}$, $\Phi = 1+P_1\sin\Lambda+P_2\cos\Lambda$, f_R, f_T, and f_N are the force components in the RTN frame [8].

4.2 Relative orbit motion

4.2.1 CWH Equations

The Clohessy-Wiltshire-Hill (CWH) equations provide a linearized solution to the relative motion problem between two nearby spacecraft in orbit. These equations assume that the chief spacecraft is in a circular orbit and that the deputy spacecraft has small relative distances and velocities with respect to the chief. They describe the relative motion in the RTN frame. The dynamics of the deputy spacecraft relative to the chief are governed by [9] the following equations

$$\begin{cases} \ddot{x} - 3\omega^2 x - 2\omega\dot{y} = 0 \\ \ddot{y} + 2\omega\dot{x} = 0 \\ \ddot{z} + \omega^2 z = 0 \end{cases} \tag{19}$$

where $\ddot{x}$, $\ddot{y}$, and $\ddot{z}$ represent the second derivatives of the deputy's position in the RTN frame, ω is the mean motion of the chief spacecraft. Rather than characterizing the relative trajectory using the cartesian coordinates in the RTN frame, an alternative definition based on the vector of orbital element differences is also used

$$\delta\mathbf{e} = (\delta a, \delta e, \delta i, \delta\Omega, \delta\omega, \delta\nu_0)^T \tag{20}$$

However, when describing a relative orbit through orbit element differences, it is not convenient to describe the anomaly difference through $\delta\nu$. To avoid this issue, the desired anomaly difference between two orbits is typically expressed as a mean anomaly difference δM.

4.2.2 Linearized relative orbit motion

In order to minimise the relative drift effect all satellites must be subject to the same $\dot{\Omega}$ and $\dot{\omega}$, therefore the difference in inclination, semi-major axis and eccentricity must be zero. Under this condition and assuming a close formation with a relative distance between a few meters to a few tens of meters, the linear relative motion equations are [10]

$$\begin{cases} x = \frac{ae\sin(\nu+\omega)\delta M}{\sqrt{1-e^2}} \\ y = \frac{r(1+e\cos\nu)^2\delta M}{(1-e^2)^{3/2}} + r\delta\omega + r\cos i\delta\Omega \\ z = -r\cos(\nu+\omega)\sin i\delta\Omega \end{cases} \tag{21}$$

where $r = \frac{a(1-e^2)}{1+e\cos\nu}$.

4.3 Attitude

4.3.1 Equation of Motion

Given the Euler angles $(\phi,\theta,\psi)^T$ and angular velocity $(p,q,r)^T$ expressed in the body frame, the variation in time of the Euler angles is given by [9]

$$\begin{cases} \frac{d\phi}{dt} = \frac{p\sin\psi+q\cos\psi}{\sin\theta} \\ \frac{d\theta}{dt} = p\cos\psi - q\sin\psi \\ \frac{d\psi}{dt} = r - (p\sin\psi+q\cos\psi)\cot\theta \end{cases} \tag{22}$$

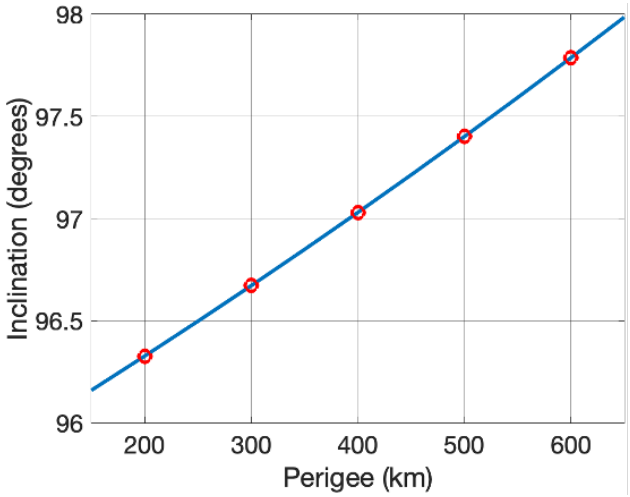

Figure 1: Inclination as a function of the altitude of perigee for an SSO.

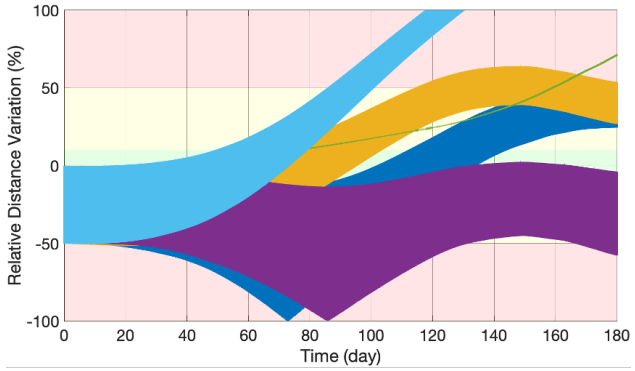

Figure 2: Relative distance variation evolution for a 500km SSO. Each color represents a CS.

The variation in time of the components of the angular velocity is given by Euler's equations

$$\begin{cases} \frac{dp}{dt} = \frac{qr(C-B)}{A} \\ \frac{dq}{dt} = \frac{rp(A-C)}{B} \\ \frac{dr}{dt} = \frac{pq(B-A)}{C} \end{cases} \tag{23}$$

where A, B, and C are the principal moments of inertia.

5 Mission Analysis

The 16U4SBSP mission aims to demonstrate SBSP using a CS swarm from Earth orbit. This demonstration employs seven 16U CSs to deliver 1 kW-scale wireless energy via RF beaming, adaptable for both space-to-ground and space-to-space applications. The primary goal is to validate SBSP provision using a satellite swarm and explore miniaturized technologies for future large-scale missions that could benefit remote or emergency areas. Firstly, the mission orbit is identified. The case of Sun-synchronous orbits (SSO) is considered. SSOs are a type of near-polar orbit that enables a satellite to pass over a given point on Earth's surface at the same local solar time. This characteristic is achieved through a precise inclination and altitude that causes the orbit's Right Ascension of the Ascending Node Ω to precess at the same rate Earth orbits around the Sun, effectively synchronizing with the solar cycle. Fig. 1 shows the SSO inclination as a function of the altitude of perigee. For missions where power is primarily needed at night to complement ground-based solar arrays, an SSO offers significant advantages. It maximizes illumination during operational periods and minimizes the energy storage requirements, as the satellites are strategically positioned to efficiently leverage sunlight. The configuration of the swarm consists of seven CSs arranged in a circular formation, with one central chief CS and six deputy CSs arranged hexagonally around it. The initial positions of each CS within the RTN frame are given by

$$\begin{cases} x_0 = 0 \\ y_0 = r\cos\lambda_i \\ z_0 = r\sin\lambda_i \end{cases} \tag{24}$$

where r is the formation radius and λ_i is the phase of the i-th CS on the circular formation. To prevent orbital element drift, every CS, both the chief and deputies, has identical semimajor axes, eccentricities, and inclinations. So, using the linearized relative motion equations, the initial values of $\Delta\Omega$, $\Delta\omega$, and ΔM are determined. The relative distance variation of each deputy CS with respect to the chief CS is defined as

$$RDV = \frac{d(t) - d(0)}{d(0)} \times 100 \tag{25}$$

where $d = |r_D - r_C|$, r_D and r_C are the norm of the deputy and chief CSs. In the following analysis, the mission is assumed to be initially at an altitude of perigee of 500 km and with $\Omega_0 = \omega_0 = M_0 = 0$. Fig. 2 shows the Relative Distance Variation (RDV) evolution of the swarm in an SSO. The RDV interval between $[-100, 100]\%$ is subdivided in three regions: $|RDV_{max}| < 10\%$ in green; $10\% < |RDV_{max}| < 50\%$ in yellow; $|RDV_{max}| > 50\%$ in red. It is observed that for the initial 20 days, the formation remains stable. The drag and SRP perturbations are characterized. Fig. 3 shows these perturbations in the

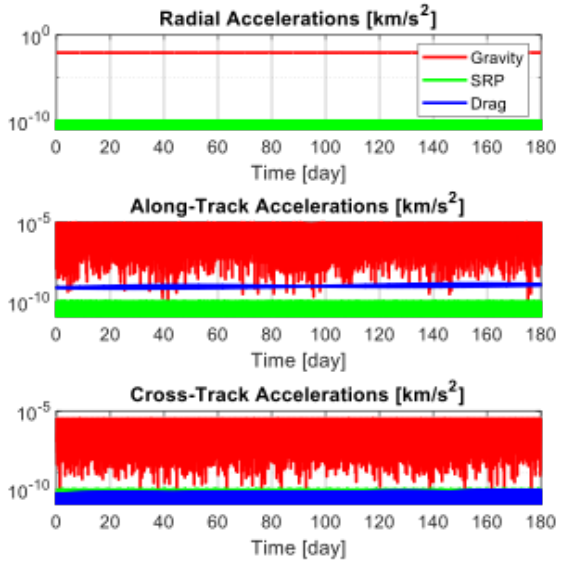

Figure 3: Orbital perturbations affecting the evolution of the formation over 6 months. The gravitational, drag and SRP perturbations are in red, blue and green respectively.

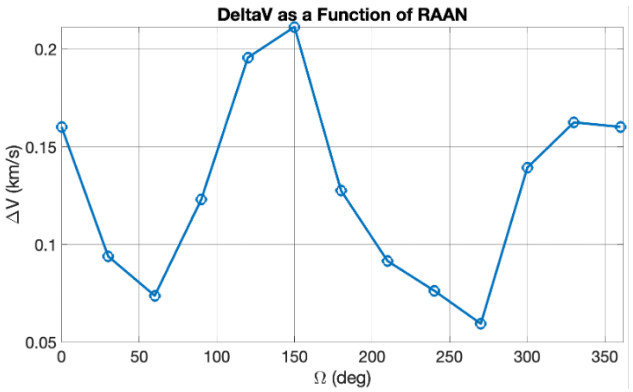

Figure 4: Δv for formation acquisition as a function of Ω_0.

RTN frame. In the radial direction, the CSs are affected by gravitational perturbation and the solar radiation pressure. In the along-track direction, the effect of the drag is added to the perturbations. For the case of 500 km, it has a larger magnitude than the SRP perturbation. In the cross-track direction, the CSs are affected by the drag component due to the atmosphere rotation. The analysis of the Δv for the formation acquisition dependence on the initial condition and launch date is conducted. Fig. 4 shows the Δv for different values of Ω_0 in the case of an SSO with an altitude of perigee of 500 km. The interval of $\Omega_0 = [0, 2\pi]$ is considered. It is observed the periodic behaviour of the Δv with respect to the initial Ω_0, where the most convenient orientations are identified to be for $\Omega_0 = 60°$ and $\Omega_0 = 270°$. Choosing $\Omega_0 = 270°$, the Δv for different launch dates is characterized and shown in Fig. 5. The launch date interval considered is between the 1st of January and the 23rd of June. Again, a periodic behaviour of the Δv is identified and the optimal launch date interval is between the 8th of February and the 8th of March. Finally, the mission CONOPS are listed.

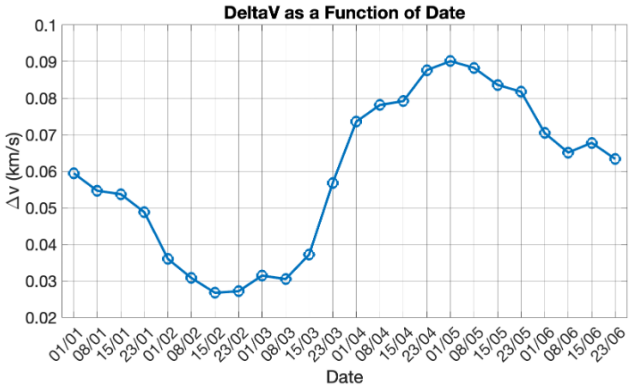

Figure 5: Δv for formation acquisition as a function of launch date.

5.1 Formation Deployment

The CSs are deployed into an SSO, with a release cadence of every 30 seconds. The provided Δv ranges from 1.6 to

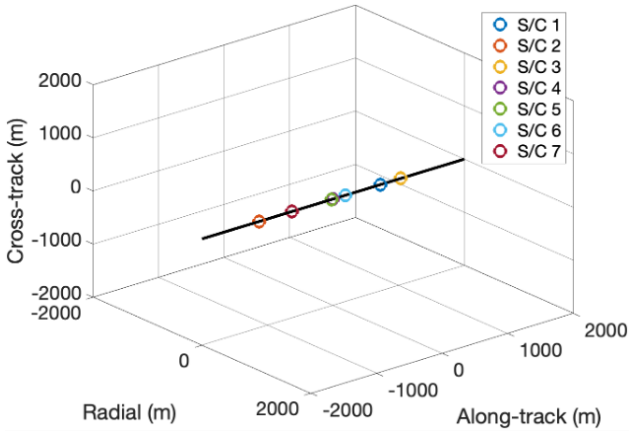

Figure 6: CS distribution in the along-track direction before formation acquisition. The black line represents the orbit segment and each coloured circle represents a single CS.

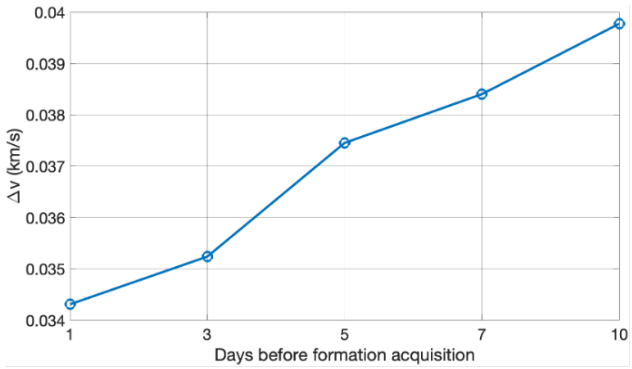

Figure 7: Average Δv to acquire the formation as a function of the observation campaign's duration.

2 m/s. The LEOP have a duration of one day for attitude acquisition, solar array deployment, and subsystem checks. Then, manoeuvres for orbit circularization and phase correction of each CS are executed to ensure that the CSs are distributed within a range of ± 1000 m from a central reference point as in Fig. 6. An observation campaign is conducted before acquiring the formation for 10 days. An analysis on the number of days to perform the observation campaigns is performed to identify the Δv required to acquire the formation after a certain number of days as shown in Fig. 7. The Δv includes all the manoeuvres from the formation deployment. The average Δv required varies between 0.0343 and 0.0398 km/s if the formation is acquired after 1 and 10 days, respectively.

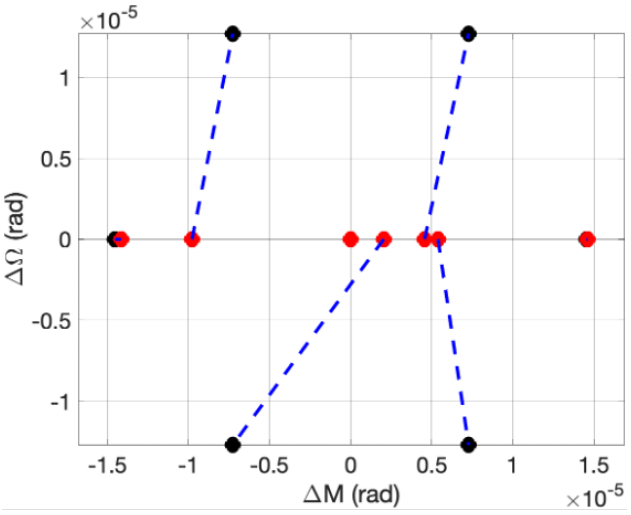

Figure 8: Formation distribution from the along-track direction (in red) to the hexagonal formation (in black). The final and initial positions in the ΔM - $\Delta\Omega$ plane of each CS are connected by a blue dashed line.

5.1.1 Formation Acquisition

A formation with a radius of 1000 meters is established as shown in Fig. 8, and two days are reserved for verifying formation control, assessing orbit/attitude perturbations, antenna pointing, and time synchronization. The following analytical formulas provide an estimation of the cost to correct each angular parameter.

$$\Delta v_\Omega = \sqrt{\frac{\mu \sin i}{a}} \Delta\Omega, \quad \Delta v_M = -\frac{an}{2} \Delta M \tag{26}$$

$$\Delta v_{\text{TOT}} = |\Delta v_\Omega| + |\Delta v_M| \tag{27}$$

In Fig. 9, the Δv required to acquire the formation is estimated. The Δv includes all the manoeuvres from the CS deployments until the 1000 m formation acquisition. In the figure, each case is characterized by a random value of Δv initially provided between 1.6 and 2 m/s. From the analysis, the average estimated Δv 0.3 m/s.

5.2 Operative Phase

The formation is then adjusted to decrease the radius to 100 meters and is maintained for the first half of the mission's duration (3 months). For the second half (3 months), the radius is further reduced to 10 meters. Initially, the analyses performed in this phase assume perfect knowledge of the CS's attitude and, later, assume uncertainty in the attitude, i.e. offset, within certain limits. The cases of maximum uncertainty of $0.1°$, $0.25°$ and $0.5°$ are

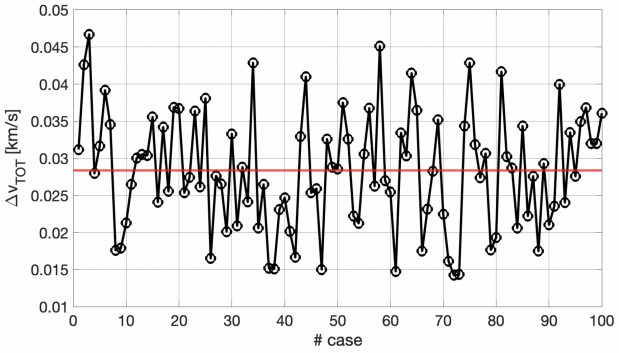

Figure 9: Total Δv for formation deployment and acquisition for 100 cases (in black) for a 100 m hexagonal formation. The red line represents the average Δv (approx. 28 m/s).

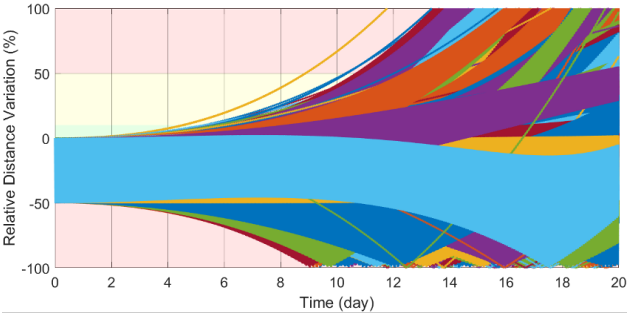

Figure 10: Evolution of the RDV for a maximum uncertainty in the CS attitude of $0.1°$.

considered. Figures 10-12 show the RDV for the first 20 days for each case. The maximum DD and DSRP in each case are analyzed and shown in Figures 13-15. For each attitude uncertainty case, a Monte Carlo analysis is performed to establish how frequently the formation must be controlled. Two scenarios are considered: the collision case considers the eventuality in which one of the deputy CS is too close (-75% RDV) to the chief CS that a correction manoeuvre must be performed; the divergence case considers the eventuality in which one of the deputy CS is too far (+50% RDV) from the chief CS. Fig. 16 shows the results of this analysis. As mentioned at the beginning of the mission analysis section, the formation in SSO is stable for the first 20 days. This was the case with perfect knowledge of the attitude, i.e. offset equal to 0. As the uncertainty increases, the formation must be controlled more frequently. From Fig. 17, it is clear that the strictest scenario is the collision one. For this reason, the control frequency is based on this case. For a maximum attitude uncertainty of $0.1°$, $0.25°$ and $0.5°$, the for-

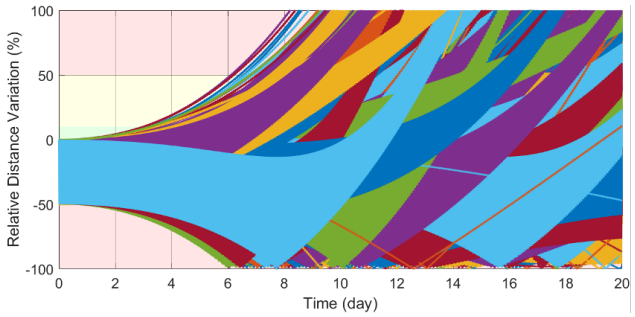

Figure 11: Evolution of the RDV for a maximum uncertainty in the CS attitude of $0.25°$.

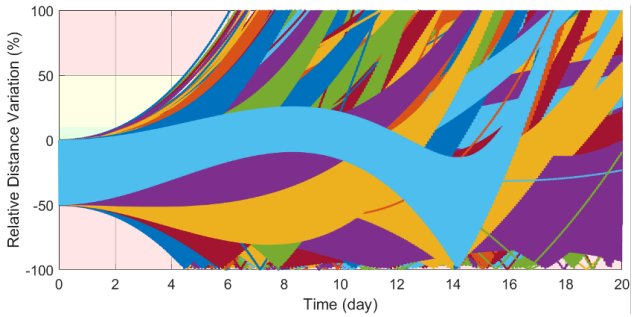

Figure 12: Evolution of the RDV for a maximum uncertainty in the CS attitude of $0.5°$.

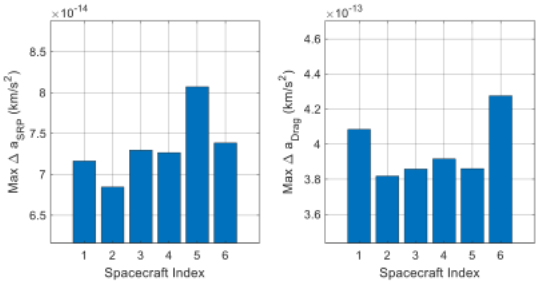

Figure 13: Maximum differential SRP (left) and drag (right) for each CS for a maximum uncertainty in the CS attitude of $0.1°$.

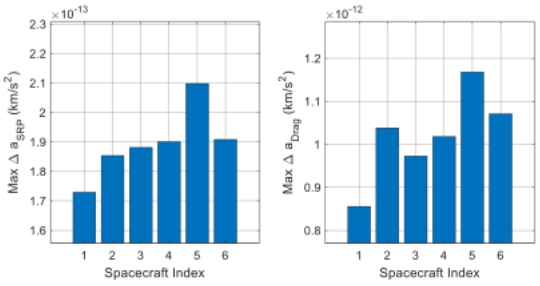

Figure 14: Maximum differential SRP (left) and drag (right) for each CS for a maximum uncertainty in the CS attitude of $0.25°$.

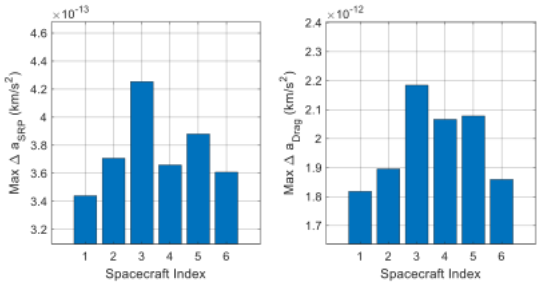

Figure 15: Maximum differential SRP (left) and drag (right) for each CS for a maximum uncertainty in the CS attitude of $0.5°$.

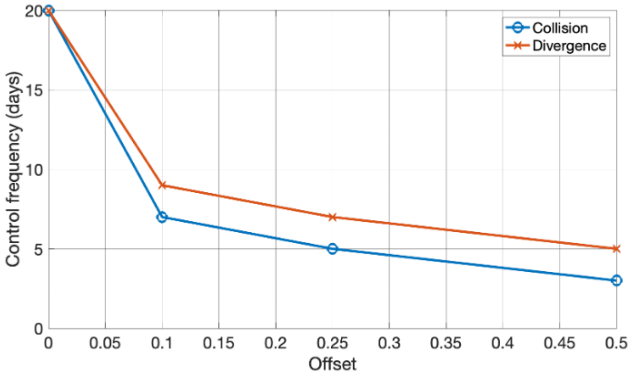

Figure 16: Number of days that the formation can be left uncontrolled as a function of the uncertainty in the attitude for a 100m formation.

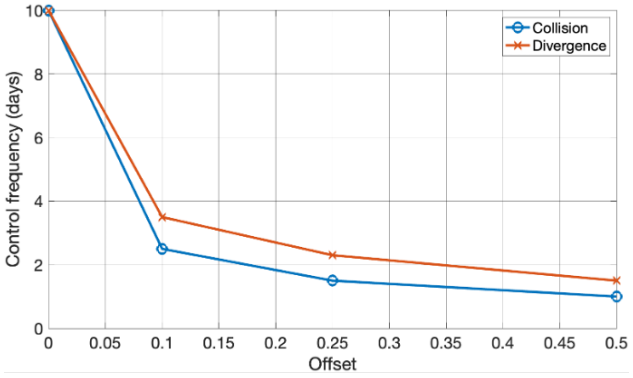

Figure 17: Number of days that the formation can be left uncontrolled as a function of the uncertainty in the attitude for a 10m formation.

mation must be controlled at maximum every 7, 5 and 3 days, respectively. Fig. 17 shows the analysis for a 10m formation. The same rationale is applied in the case of a 10m formation. For a maximum attitude uncertainty of $0.1°$, $0.25°$ and $0.5°$, the formation must be controlled at a maximum every 2.5, 1.5 and 1 day, respectively. Depending on mission requirements, throughout our analysis, the formation is controlled more frequently. The relative positioning of the CS swarm is managed through a bang-bang limit-cycle controller. Generally, this type of controller operates by switching full-on or full-off actuator inputs, such as thrusters, in response to the position of the CS. In the context of this mission, when a predetermined time interval has passed, the controller activates the actuators to provide a maximum force in one direction until the state variables are restored to the initial values. The controller's simplicity is advantageous for the limited computational resources available on small satellites like CSs. Fig. 18 shows the evolution of the Δv to maintain the formation throughout the mission duration for each CS.

5.3 End-of-Life phase

Finally, the mission is concluded in compliance with the ESA's Space Debris Mitigation Requirements, which require re-entry within 5 years. For an initial altitude of 500 km, the mission is projected to naturally re-enter the Earth's atmosphere within 1.5 years, as shown in Fig. 19. Similarly, the analysis is extended to the altitudes of 600 and 700 km and the results, in terms of Δv required for each mission phase, are presented in the next section.

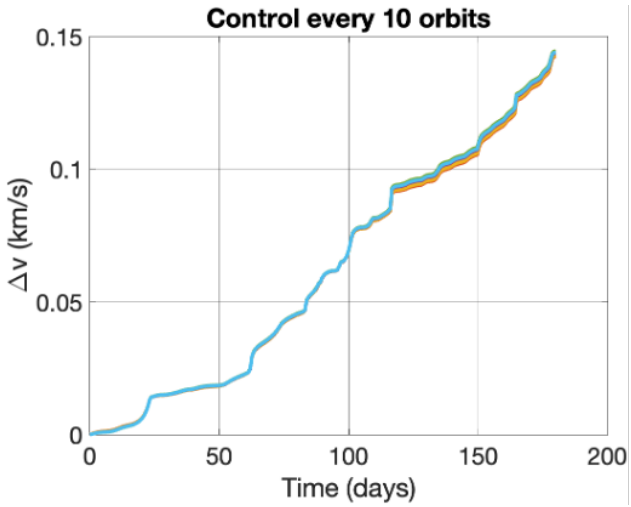

Figure 18: Δv to maintain the formation for 6 months. The formation is controlled every 10 days.

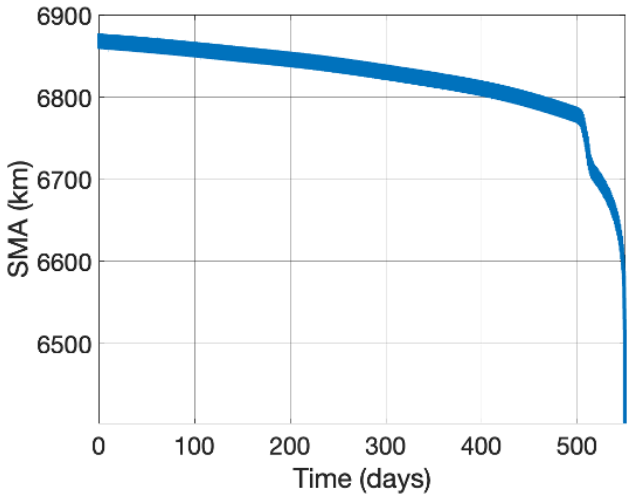

Figure 19: Semimajor axis evolution in the End-of-Life phase.

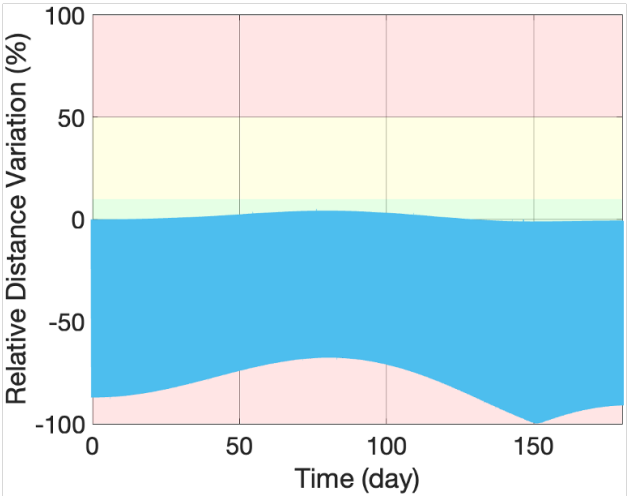

Figure 20: RDV for $h = 500$ km for an SSO midday/midnight orbit.

6 Mission baseline

To satisfy the mission's illumination requirements [11], the reference case is found unsuitable. After thorough analysis, a midday/midnight SSO with $\Omega_0 = 280°$ is chosen. Fig. 20 shows the RDV for $h = 600$ km. It is noteworthy that the formation shape is preserved for six months despite orbital perturbations, unlike the previous case (refer to Fig. 2) where the formation was maintained for only 20 days, saving on total Δv budget. This is crucial, as the Δv budget increases significantly once the antenna is deployed. In previous analyses, it was assumed that the antenna was not deployed, but each CS will need to deploy its antenna after reaching the final orbit. The analysis will now be performed with the antenna deployed for the entire mission. With the antenna deployed, the A/m increases, making the formation more susceptible to orbital perturbations, leading to re-entry much before the mission's end. Specifically,

- For $h = 500$ km, the re-entry is in 15 days (see Fig. 21);
- For $h = 600$ km, the re-entry is in 90 days;
- For $h = 700$ km, the formation does not re-enter.

A trade-off analysis between re-entry time and the total Δv budget yields the following options

- If $h = 500$ km is chosen the semimajor axis is corrected every 10 days (at 450 km), and each manoeuvre will cost 28 m/s. For 6 months is 504 m/s and 1008 m/s for one year.

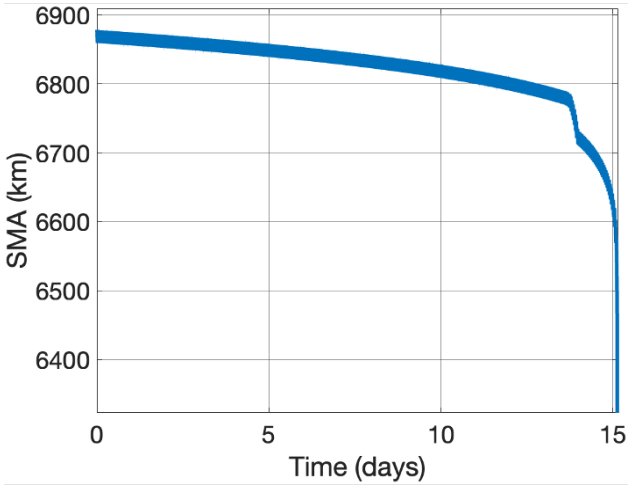

Figure 21: Semi-major axis evolution for the case of antenna deployed and $h = 500$ km.

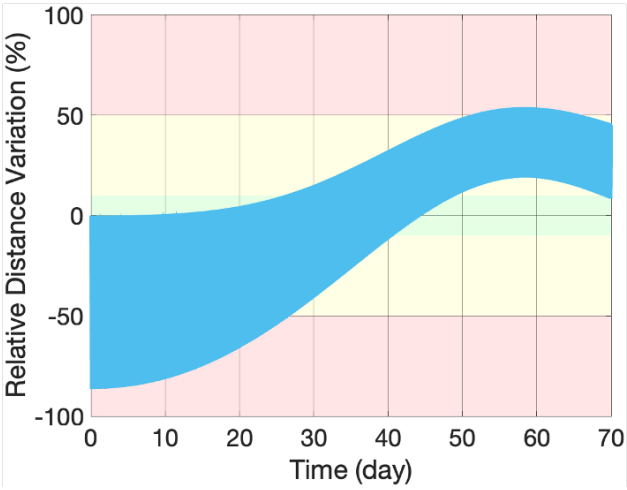

Figure 22: RDV for the case of antenna deployed at $h = 600$ km for 70 days.

- If $h = 600$ km is chosen the semimajor axis is corrected every 70 days (at 500 km), and each manoeuvre will cost 55 m/s. For 6 months is 137 m/s and 274 m/s for one year.
- If $h = 600$ km is chosen the semimajor axis is corrected every 45 days (at 550 km), and each manoeuvre will cost 28 m/s. For 6 months is 112 m/s and 224 m/s for one year.
- If $h = 700$ km is chosen, no semimajor axis correction within one year. However, to have a smaller beaming footprint on ground, lower altitudes are preferred.

As a result, $h = 600$ km is chosen as a trade-off between the Δv budget and beaming footprint. Fig. 22 shows the RDV evolution in a midday/midnight orbit at 600 km with the hexagonal antenna deployed. Despite the antenna deployment altering the RDV evolution, the formation shape is preserved for 70 days without maneuvering. After 70 days, the RDV re-enters the "green zone," reducing the Δv needed to correct the orbit. The previous analysis is adapted considering the antenna deployment, and the table in Fig. 23 summarizes the results for different altitudes: 500 km, 600 km, and 700 km SSOs. This analysis highlights the advantage of choosing a 600 km midday/midnight SSO. Although this option requires approximately 34% more Δv compared to a 700 km SSO, its smaller beaming footprint makes it more advantageous. Additionally, it is clearly more convenient than the 500 km and 600 km SSOs.

7 Conclusion

The 16U4SBSP mission, one of the selected concepts of the ESA SysNova challenge "Innovative Missions Concepts enabled by Swarms of CubeSats", has the primary objective to validate, with a small-scale mission, the beamforming power transmission model developed by the mission consortium and, in this way, confirm that it is feasible and convenient to provide SBSP using a larger constellation of spacecraft. This paper provides a preliminary analysis of the dynamics involved in the 16U4SBSP mission, aimed at demonstrating SBSP using a CS swarm. Key findings from the mission analysis reveal the impact of gravitational perturbations, solar radiation pressure, and atmospheric drag on the spacecraft dynamics. The selection of an SSO is justified for optimal power generation and efficiency in power delivery. The study highlights the necessity of optimal launch dates and initial conditions to minimize Δv requirements across various mission phases, thus reducing propellant use. The analysis of the operative phase under different degrees of attitude uncertainty emphasizes the importance of precise formation control to ensure mission objectives are met. The End-of-Life phase analysis demonstrates compliance with space debris mitigation guidelines, highlighting the mission's sustainability. Finally, it is found that a midday/midnight SSO at an altitude of 600 km is suitable for the mission, which is presented as the baseline for the 16U4SBSP mission concept.

Phases	Δv [km/s] (500 km)	Δv [km/s] (600 km)	Δv [km/s] (600 km) midday orbit	Δv [km/s] (700 km)
Formation acquisition	0.04 (avg) 0.075 (max)	0.030 (avg) 0.068 (max)	0.030 (avg) 0.068 (max)	0.03 (avg) 0.066 (max)
Operative phase	1.1 (offset = 0) 1.26 (offset = 0.5)	0.32 (offset = 0) 0.454 (offset = 0.5)	0.274	0 (offset = 0) 0.16 (offset = 0.5)
End-of-life phase	0 (re-entry in 15 days since last orbit correction maneuver)	0 (re-entry in 90 days since last orbit correction maneuver)	0 (re-entry in 90 days since last orbit correction maneuver)	0 (re-entry in 13 months since last orbit correction maneuver)
Δv_{TOT}	1.335	0.522	0.342	0.226

Figure 23: Δv budget for every mission phase considering initial altitudes of 500, 600, and 700 km for a mission duration of 1 year.

References

[1] ESA, "SoW Innovative Mission Concepts Enabled by Swarms of CubeSats – OSIP Campaign," 2023, ESA-TECSF-SOW-2023-001164.

[2] H. D. Curtis, *Orbital Mechanics for Engineering Students*, 2014.

[3] W. Kaula, *Theory of satellite geodesy: applications of satellites to geodesy*, 1996.

[4] C. Benson and D. Scheeres, "Averaged solar torque rotational dynamics for defunct satellites," *Journal of Guidance, Control, and Dynamics*, vol. 44, no. 4, 2021.

[5] V. V. Beletsky, "Motion of an artificial satellite about its center of mass," NASA, Nasa technical documents, 1966.

[6] D. A. Vallado, *Fundamentals of Astrodynamics and Applications*, ser. Space Technology Library, 1997.

[7] R. H. Battin, *An introduction to the Mathematics and Methods of Astrodynamics*, ser. AIAA Education Series, New York, 1999.

[8] M. D. Carlo, S. da Graca Marto, and M. Vasile, "Extended analytical formulae for the perturbed keplerian motion under low-thrust acceleration and orbital perturbations," *Celestial Mechanics and Dynamical Astronomy*, vol. 133, no. 3, p. 13, 2021.

[9] H. Schaub and J. L. Junkins, *Analytical Mechanics of aerospace systems*, 2002.

[10] M. Vasile, "Fractioned solar power satellite for regional coverage," in *63rd International Astronautical Congress*, Naples, Italy, 2012.

[11] A. Cervone *et al.*, "Phase-0 design of the 16u4sbsp spacecraft: a scaled demonstration of space-based solar power in earth orbit using a swarm of cubesats," in *IAF 75th International Astronautical Congress*, Milano, Italy, 2024.